A Context-Sensitive Technique for Unsupervised Change Detection Based on Hopfield-Type Neural Networks

Susmita Ghosh, Lorenzo Bruzzone, *Senior Member, IEEE*, Swarnajyoti Patra, Francesca Bovolo, *Member, IEEE*, and Ashish Ghosh

***Abstract*—In this paper, we propose a context-sensitive technique for unsupervised change detection in multitemporal remote sensing images. This technique is based on a modified Hopfield neural network architecture designed to model spatial correlation between neighboring pixels of the difference image produced by comparing images acquired on the same area at different times. Each spatial position in the considered scene is represented by a neuron in the Hopfield network that is connected only to its neighboring units. These connections model the spatial correlation between neighboring pixels and are associated with a context-sensitive energy function that represents the overall status of the network. Change detection maps are obtained by iteratively updating the output status of the neurons until a minimum of the energy function is reached and the network assumes a stable state. A simple heuristic thresholding procedure is presented and adopted for initializing the network. The proposed change detection technique is unsupervised and distribution free. Experimental results carried out on two multispectral and multitemporal remote sensing images confirm the effectiveness of the proposed technique.**

***Index Terms*—Change detection, context-sensitive image analysis, Hopfield neural network, multitemporal images, remote sensing, thresholding.**

I. Introduction

IN REMOTE sensing applications, change detection is the process aimed at identifying differences in the state of a land cover by analyzing a pair of images acquired on the same geographical area at different times [1], [2]. Such a problem plays an important role in many different domains like studies on land use/land cover dynamic [3], monitoring shifting cultivations [4], burned areas identification [5], analysis of deforestation processes [6], [7], assessment of vegetation changes [8], and monitoring of urban growth [9]. Since all of these applications usually require an analysis of large areas, development of completely automatic and unsupervised change detection techniques is of high relevance to reduce the time effort required by manual image analysis and to produce objective change detection maps.

In the literature, the most widely used unsupervised change detection techniques are based on a three-step procedure [1], namely 1) preprocessing, 2) pixel-by-pixel comparison of two multitemporal images, and 3) image analysis. The aim of the preprocessing step is to make the considered images as comparable as possible and includes operations like coregistration, radiometric and geometric corrections, and noise reduction. The comparison step aims at producing a further image, where differences between the two considered acquisitions are highlighted. Different mathematical operators can be adopted to perform image comparison. When dealing with optical images, the most widely used operator is the difference. This operator can be applied to: 1) a single spectral band (univariate image differencing) [1], [10], [11]; 2) multiple spectral bands [change vector analysis (CVA)] [1], [12]; and 3) vegetation indexes (vegetation index differencing) [1], [13] or other linear (e.g., tasseled cap transformation [10]) or nonlinear combinations of spectral bands. Each choice gives rise to a different technique. Among these, the most popular is the CVA that computes the difference image as the magnitude of spectral change vectors obtained for each pair of corresponding pixels by vector subtraction. Once image comparison is performed, the change detection process can be carried out adopting either context-insensitive or context-sensitive procedures. The most widely used context-insensitive analysis techniques are based on image thresholding. The decision threshold can be selected either with a manual trial-and-error procedure (according to a desired tradeoff between false and missed alarms) or with automatic techniques (e.g., by analyzing the statistical distribution of the image obtained after comparison, by fixing the desired false alarm probability, or following a Bayesian minimum error decision rule [12]). The mentioned thresholding procedures do not take into account the spatial correlation between neighboring pixels in the decision process, i.e., they implicitly assume that the image has an impulsive autocorrelation function. To overcome this limitation of neglecting the interpixel class dependence, a context-sensitive change detection procedure based on Markov random field (MRF) has been proposed in [12].

The aforementioned context-sensitive and context-insensitive automatic approaches to change detection require the selection of a proper model for the statistical distributions of changed and unchanged pixels. To obtain an unsupervised estimation of the parameters of the statistical models describing the class distributions, techniques based on the Expectation–Maximization (EM) algorithm can be used [14].

Manuscript received April 7, 2006; revised October 6, 2006.

S. Ghosh and S. Patra are with the Department of Computer Science and Engineering, Jadavpur University, Kolkata 700032, India (e-mail: susmita_de@rediffmail.com).

L. Bruzzone and F. Bovolo are with the Department of Information and Communication Technology, University of Trento, 38050 Trento, Italy (e-mail: lorenzo.bruzzone@ing.unitn.it).

A. Ghosh is with the Machine Intelligence Unit and Center for Soft Computing Research, Indian Statistical Institute, Kolkata 700108, India (e-mail: ash@isical.ac.in).

Digital Object Identifier 10.1109/TGRS.2006.888861

In change detection problems of remote sensing images, the EM algorithm has been formulated under different assumptions for class distributions, i.e., Gaussian [12], generalized Gaussian [15], and mixture of Gaussians [16].

To overcome the limitations imposed by the need of selecting a statistical model for change and no-change class distributions, in this paper, we propose an unsupervised and context-sensitive change detection technique, which is distribution free. The presented algorithm automatically detects the changes in the difference image using the collective computational ability of a Hopfield-type neural network [17]. The specific architecture of the Hopfield network used in this paper considers contextual information from the neighborhood of each pixel to generate an accurate change detection map. In the presented architecture, each neuron corresponds to a pixel of the difference image and is connected to all the neurons in the neighborhood. Given an initial state, the status of each neuron is modified iteratively. When the network reaches a stable state (local minimum of its energy function), the difference image is classified into two classes (neurons having ON $(+1)$ status represent the changed pixels and those having OFF (-1) status represent the unchanged pixels). The major advantages of the proposed technique are listed as follows: 1) it is distribution free (both the proposed initialization strategy of the network and the energy function adopted are not based on any specific parametric model for the distributions of classes); 2) it properly exploits the spatiocontextual information making the change detection process robust to isolated noisy patterns (the procedure for updating the status of the neurons is regularized by the information included in the neighborhood); 3) it is completely unsupervised (the proposed initialization strategy does not require any *a priori* information); and 4) unlike the technique proposed in [12], it does not require manual setting of any input parameter.

To assess the effectiveness of the presented technique, we considered two real multitemporal remote sensing data sets and compared the results provided by the proposed technique with those obtained by reference methods published in the literature.

This paper is organized as follows: Section II provides a brief description of the Hopfield neural network. Section III describes the proposed change detection technique. The data sets used in the experiments and the obtained results are described in Section IV. Finally, in Section V, conclusions are drawn.

II. Background: Hopfield Neural Networks

A Hopfield neural network consists of a set of neurons (or units). The output of each neuron is fed back to each of the other units in the network, as illustrated in Fig. 1. There is no self-feedback loop, and the synaptic weights are symmetric [18]. Hopfield defined the energy function of the network by using the network architecture, i.e., the number of neurons, their output functions, threshold values, connection between neurons, and the strength of the connections [19]. Thus, the energy function represents the complete status of the network. Hopfield has also shown that, at each iteration of the processing of the network, the energy value decreases and the network reaches a stable state when its energy value reaches a minimum [20], [21]. Since there are interactions among all the units, the collective property inherently reduces the computational complexity.

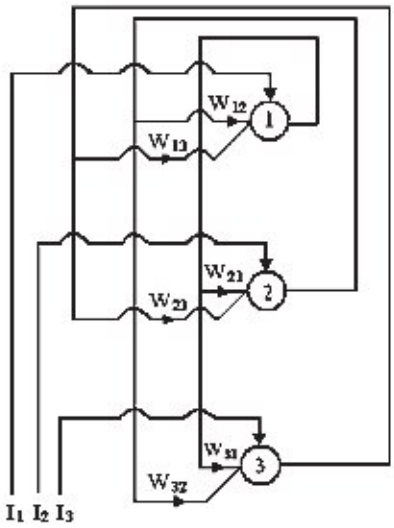

Fig. 1. Example of a Hopfield network consisting of three neurons. Neurons are represented by circles, and connected lines between neurons show that the output of each neuron is fed back to other neurons.

The input U_i to the generic ith neuron comes from two sources, namely 1) input V_j from other units (to which it is connected) and 2) external input bias I_i, which is a fixed bias applied externally to the unit i. Thus, the total input to a neuron i is given by

$$U_i = \sum_{j=1, j\neq i}^{n} W_{ij} V_j + I_i \tag{1}$$

where the weight W_{ij} represents the synaptic interconnection strength from neuron j to neuron i, and n is the total number of units in the network. The connection strengths are assumed to be symmetric, i.e., $W_{ij} = W_{ji}$. The output V_i of neuron i is defined as

$$V_i = g(U_i) \tag{2}$$

where $g(\cdot)$ is an activation function. There are two types of Hopfield models (i.e., discrete and continuous), which differ on the output values a neuron can take.

A. Discrete Model

In the discrete model, neurons are bipolar, i.e., the output V_i of neuron i is either $+1$ or -1. In this model, the activation function $g(\cdot)$ is defined according to the following threshold function:

$$V_i = g(U_i) = \begin{cases} +1, & \text{if } U_i \geq \theta_i \\ -1, & \text{if } U_i < \theta_i \end{cases} \tag{3}$$

where θ_i is the predefined threshold of neuron i. The energy function E of the discrete model is given by [20]

$$E = -\sum_{i=1}^{n} \sum_{j=1, i\neq j}^{n} W_{ij} V_i V_j - \sum_{i=1}^{n} I_i V_i + \sum_{i=1}^{n} \theta_i V_i. \tag{4}$$

The change of energy ΔE due to a change of output state of the neuron i equal to ΔV_i is

$$\Delta E = -\left[\sum_{j=1, i\neq j}^{n} W_{ij}V_j + I_i - \theta_i\right]\Delta V_i = -[U_i - \theta_i]\Delta V_i. \tag{5}$$

If ΔV_i is positive (i.e., the state of the neuron i is changed from -1 to $+1$), then from (3) we can see that the bracketed quantity in (5) is also positive, making ΔE negative. When ΔV_i is negative (i.e., the state of the neuron i is changed from $+1$ to -1), then from (3) we can see that the bracketed quantity in (5) is also negative. Thus, any change in E according to (3) is negative. Since E is bounded, the time required by the system to reach convergence is associated to a motion in the state space that seeks out minima of E and stops at such points.

B. Continuous Model

In this model, the output of a neuron is continuous [21] and can assume any real value between $[-1, +1]$. In the continuous model, the activation function $g(\cdot)$ must satisfy the following conditions: 1) it is a monotonic nondecreasing function and 2) $g^{-1}(\cdot)$ exists.

A typical choice of the function $g(\cdot)$ is

$$g(U_i) = \frac{2}{1 + e^{-\phi_i(U_i - \tau)}} - 1 \tag{6}$$

where the parameter τ controls the shifting of the sigmoidal function $g(\cdot)$ along the abscissa, and ϕ_i determines the steepness (gain) of neuron i. The value of $g(U_i)$ lies in $[-1, +1]$ and is equal to 0 at $U_i = \tau$. The energy function E of the continuous model is given by [21]

$$E = -\sum_{i=1}^{n}\sum_{j=1, i\neq j}^{n} W_{ij}V_iV_j - \sum_{i=1}^{n} I_iV_i + \sum_{i=1}^{n}\frac{1}{R_i}\int_0^{V_i} g^{-1}(V_i)dV. \tag{7}$$

The function E is a Lyapunov function, and R_i is the total input impedance of the amplifier realizing a neuron i. It can be shown that when neurons are updated according to (6), any change in E is negative. The last term in (7) is the energy loss term, which becomes zero at the high gain region. If the gain of the function becomes infinitely large (i.e., the sigmoidal nonlinearity approaches the idealized hard-limiting form), the last term will become negligibly small. In the limiting case, when $\phi_i = \infty$ for all i, the maxima and minima of the continuous model become identical to those of the corresponding discrete Hopfield model. In this case, the energy function is simply defined by

$$E = -\sum_{i=1}^{n}\sum_{j=1, i\neq j}^{n} W_{ij}V_iV_j - \sum_{i=1}^{n} I_iV_i \tag{8}$$

where the output state of each neuron is ± 1. Therefore, the only stable points of the very high-gain continuous deterministic Hopfield model correspond to the stable points of the discrete stochastic Hopfield model [18].

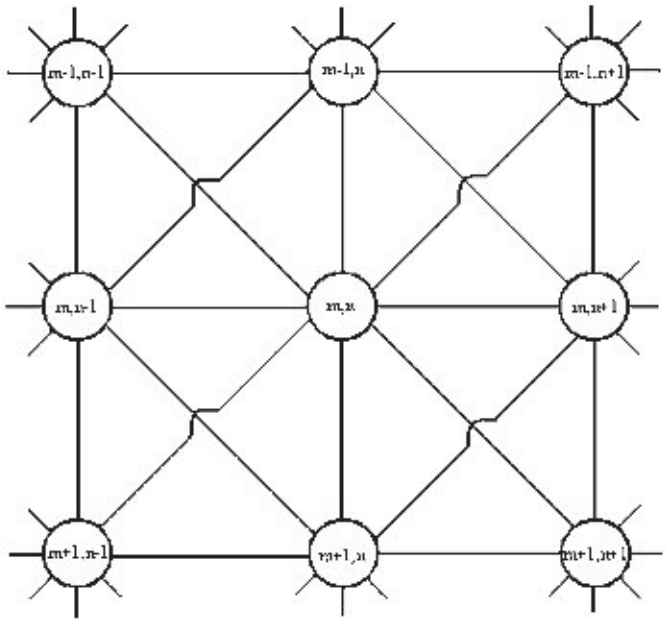

Fig. 2. Second-order topological network. Each neuron in the network is connected only to its eight neighbors. Neurons are represented by circles, and lines represent connections between neurons.

III. Proposed Change Detection Technique Based on a Modified Hopfield Neural Network Architecture

A. Description of the Network Architecture

Let us consider two coregistered and radiometrically corrected multispectral images X_1 and X_2 of size $p \times q$, acquired over the same area at different times T_1 and T_2, and let $D = \{l_{mn},\ 1 \leq m \leq p,\ 1 \leq n \leq q\}$ be the difference image obtained by applying the CVA technique to X_1 and X_2. To use Hopfield networks for solving the change detection problem, we assign to each spatial position $(m, n) \in D$ a neuron of the network. The spatial correlation between neighboring pixels is modeled by defining the spatial neighborhood systems N of order d, for a given spatial position (m, n) as $N^d_{mn} = \{(m, n) + (u, v), (u, v) \in N^d\}$. The neuron in position (m, n) is connected to its neighboring units included in N^d. According to the value of d, the neighborhood system assumes different configurations. Here, only the first- and second-order neighborhood systems have been considered, i.e., $N^1 = \{(\pm 1, 0), (0, \pm 1)\}$ and $N^2 = \{(\pm 1, 0), (0, \pm 1), (1, \pm 1), (-1, \pm 1)\}$. Fig. 2 depicts a second-order (N^2) topological network. Let $W_{mn,uv}$ be the connection strength between the (m, n)th and (u, v)th neurons. We assume that $W_{mn,uv} = 1$ if $(u, v) \in N^d_{mn}$; otherwise, $W_{mn,uv} = 0$. Hence, the presented architecture can be seen as a modified version of the Hopfield network [17] in which the connection strength to all neurons outside the neighborhood (N^d) is zero. As each neuron is connected only to its neighboring units, the output of a neuron depends only on its neighboring elements. In this way, the network architecture is intrinsically able to model and properly consider the spatio-contextual information of each pixel.

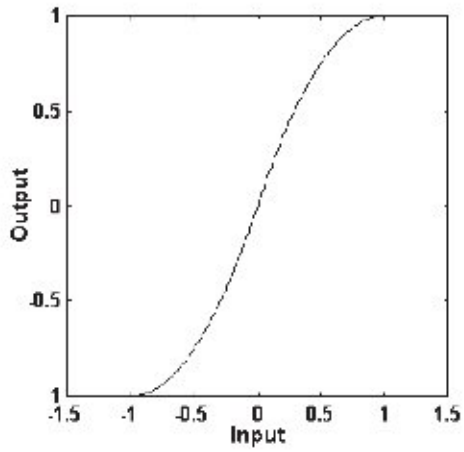

Fig. 3. Behavior of the activation function defined in $[-1, +1]$, assuming $r = 2$.

From (6), we note that the output V_{mn} for the neuron at position (m, n) is given by

$$V_{mn} = \lim_{U_{mn} \to \infty} g(U_{mn}) = +1$$
$$V_{mn} = \lim_{U_{mn} \to -\infty} g(U_{mn}) = -1.$$

Thus, the domain of U_{mn} is $(-\infty, +\infty)$. To simplify the problem, here we use the generalized fuzzy S-function [17], [22] defined over a finite domain as input/output transfer function (activation function). The form of the S-function is given as follows:

$$V_{mn} = g(U_{mn}) = \begin{cases} -1, & U_{mn} \le a \\ 2^r \left\{ \frac{(U_{mn}-a)}{(c-a)} \right\}^r - 1, & a \le U_{mn} < b \\ 1 - 2^r \left\{ \frac{(c-U_{mn})}{(c-a)} \right\}^r, & b \le U_{mn} \le c \\ 1, & U_{mn} \ge c \end{cases} \tag{9}$$

where $r \ge 2$, and $b = (a + c)/2$. In this case, $g(U_{mn})$ lies in $[-1, +1]$ with $g(U_{mn}) = 0$ at $U_{mn} = b$. The domain of U_{mn} is $[a, c]$. The value of r tunes the sharpness (steepness) of the function. If the number of neighbors is eight, the input value to a neuron lies in $[-9, +9]$, i.e., $a = -9$, and $c = 9$. However, for quick convergence, one can use the domain of U_{mn} in $[-1, +1]$ and an activation function $g(\cdot)$ (which is shown in Fig. 3) is defined as follows:

$$V_{mn} = g(U_{mn}) = \begin{cases} -1, & U_{mn} \le -1 \\ (U_{mn}+1)^r - 1, & -1 \le U_{mn} \le 0 \\ 1 - (1 - U_{mn})^r, & 0 \le U_{mn} \le 1 \\ 1, & U_{mn} \ge 1. \end{cases} \tag{10}$$

B. Definition of the Energy Function for Change Detection

The aim of the presented neural architecture is to separate changed pixels from unchanged pixels in D. To accomplish this task, we should define the energy function of the network in such a manner that when the network reaches the stable state the changed regions are clearly separated from the unchanged areas. The basic idea exploited in the proposed approach is inspired by the energy function of the Hopfield model formulated for object background classification in [17].

Let us consider the energy function defined in (4) that has three parts: The first part models the local field (or feedback), whereas the second and third parts correspond to the input bias I_i and the threshold value θ_i of each neuron in the network, respectively. In terms of images, the first part can be seen as the impact of the gray values of the neighboring pixels on the energy function, whereas the second and the third parts can be attributed to the gray value of the pixel under consideration. Let us assume, without loss of generality, that the output value of each neuron lies in $[-1, +1]$. Then, the energy function can be defined in the following way: if the output of a neuron at position (m, n) is $+1$, then it corresponds to a pixel that belongs to the changed area, whereas if the output is -1, then it corresponds to a pixel that belongs to the unchanged area. Thus, the threshold between the changed and unchanged pixels can logically be taken as 0 [i.e., $\theta_{mn} = 0\ \forall(m, n)$]. This helps us to omit the third part of the energy expression [see (4)]. Each neuron at position (m, n) has an input bias I_{mn}, which can be set proportional to the actual gray value of the corresponding pixel. If the gray value of a pixel is high (low), the corresponding intensity value of the scene is expected to be high (low). The input bias value is taken in the range $[-1, +1]$. If a neuron has a very high positive bias (close to $+1$) or very high negative bias (close to -1), then it is very likely that in the stable state the output will be $+1$ or -1, respectively. Thus, the product $I_{mn}V_{mn}$ should contribute less toward the total energy value, and the second part of the energy expression may be written as

$$-\sum_{m=1}^{p}\sum_{n=1}^{q} I_{mn}V_{mn}.$$

Depending on the nonimpulsive autocorrelation function of the difference image D, we can assume that the gray value of a pixel is highly influenced by the gray values of its neighboring pixels. Thus, if a pixel belongs to a changed region, the probability that its neighboring pixels belong to the same region is very high. This suggests that if a pair of adjacent pixels have similar output values, then the energy contribution of this pair of pixels to the overall energy function should be relatively small. If the gray values of two adjacent pixels (m, n) and (u, v) are given by V_{mn} and V_{uv}, then a reasonable choice for the contribution of each of these pairs to the overall energy function is $-W_{mn,uv}V_{mn}V_{uv}$. Thus, taking into account the contribution of all pixels, the total energy can be written as

$$\begin{aligned} &-\sum_{m=1}^{p}\sum_{n=1}^{q}\sum_{(u,v)\in N_{mn}^{d}} W_{mn,uv}V_{mn}V_{uv} \\ &= -\sum_{m=1}^{p}\sum_{n=1}^{q}\left(\sum_{(u,v)\in N_{mn}^{d}} W_{mn,uv}V_{uv}\right)V_{mn} \\ &= -\sum_{m=1}^{p}\sum_{n=1}^{q} h_{mn}V_{mn} \end{aligned} \tag{11}$$

where h_{mn} is termed as the local field and models the neighborhood information of each pixel of D in the energy function. On the basis of the aforementioned analysis, the expression of the energy function can be written as

$$E = -\sum_{m=1}^{p}\sum_{n=1}^{q}\sum_{(u,v)\in N_{mn}^{d}} W_{mn,uv}V_{mn}V_{uv} - \sum_{m=1}^{p}\sum_{n=1}^{q} I_{mn}V_{mn}. \tag{12}$$

The minimization of (12) results in a stable state of the network in which changed areas are separated from unchanged ones. The energy function in (12) can be minimized by both the discrete and the continuous models.

In the case of the discrete model, both the initial external input bias I_{mn} and the input U_{mn} to a neuron are taken as $+1$ if the gray value of the corresponding pixel of D is greater than a specific global initialization threshold value t; otherwise, they have a value of -1. As the threshold t is used to set the initial value of each neuron, we call it initialization threshold (note that this initialization threshold t and the threshold θ_i defined in Section II-A are different). Here, the status updating rule is the same as in (3) with the threshold value $\theta_{mn} = 0\ \forall(m,n)$.

In the case of the continuous model, both the initial external input bias and the input to a neuron at position (m,n) are proportional to $(l_{mn}/t) - 1$ (if $(l_{mn}/t) - 1 > 1$ then the value $+1$ is used for initializing the corresponding neuron). The activation function defined in (10) is used to update the status of the network iteratively, until the network reaches the stable state. When the network reaches the stable state, we consider the value of the gain parameter $r = \infty$ (i.e., the sigmoidal nonlinearity approaches the idealized hard-limiting form) and update the network. This makes the continuous model behave like a discrete model; thus, at the stable state, the energy value of the network can be expressed according to (12).

For both the discrete and the continuous models, at each iteration itr, the external input bias $I_{mn}(itr)$ of the neuron at position (m,n) updates its value by taking the output value $V_{mn}(itr-1)$ of the previous iteration. When the network begins to update its state, the energy value is gradually reduced until the minimum (stable state) is reached. Convergence is reached when $(dV_{mn})/dt = 0\ \forall(m,n)$ [21], i.e., if for each neuron it holds that $\Delta V_{mn} = V_{mn}(itr-1) - V_{mn}(itr) = 0$.

C. Proposed Technique for a Proper Initialization of the Network

In the literature [17], the initialization of the neurons of a Hopfield network is usually carried out in a very simple way, i.e., if L is the maximum gray value of the considered image, the global initialization threshold t is fixed to $L/2$. In the discrete case, the neurons are initialized to $+1$ if the gray value of the corresponding pixel is greater than the initialization threshold value $(L/2)$; otherwise, the neurons take the value of -1. In the continuous case, a linear transform function like $2(l_{mn}/L) - 1$ is used to initialize the units in the range $[-1,+1]$. In our change detection problem, this is not a valid approach because there is no direct relation between the optimal initialization threshold value t_0 (which should be related to the minimum error in classifying changed and unchanged pixels of D) and the maximum gray value of D. To obtain a proper initialization threshold value, a possible strategy is to adopt any of the pixel-based automatic threshold selection procedures proposed in the change detection literature [12]. However, to have a distribution-free initialization strategy (which is not based on an explicit model of the distributions of changed and unchanged classes), in the proposed technique, we exploit the following simple heuristic procedure.

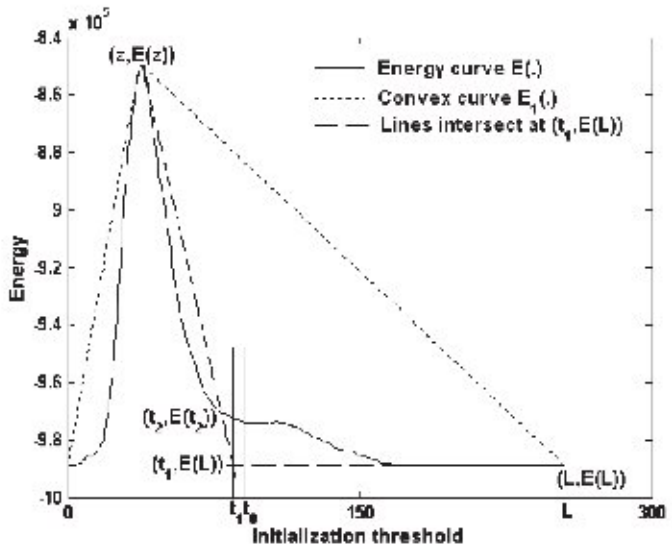

Fig. 4. Behavior of the energy value versus the initialization threshold value. The automatically detected (by the proposed heuristic approach) threshold value t_1 is close to the optimal threshold value t_0.

From (12), we can see that the energy value is minimum when V_{mn} are either all $+1$ or all $-1\ \forall(m,n)$, i.e., the whole output image belongs either to changed or unchanged areas. In the proposed procedure, we first compute the energy at convergence for various threshold values (see Fig. 4). By analyzing the behavior of this graph, one can see that initially the energy increases with initialization threshold as the number of regions (changed and unchanged) increases. After a certain threshold value, the energy decreases as the number of regions decreases (some unchanged regions are merged together). After that, the energy does not change significantly by increasing the threshold value, i.e., changed and unchanged regions are not significantly altered by the specific range of values considered. We expect that this stable behavior of the energy function is reached around the optimal initialization threshold t_0 (see Fig. 4). If the threshold value increases more, the energy changes slowly and reaches a minimum when the whole output image belongs to the class of unchanged areas. By observing this general behavior, we propose a heuristic technique that generates the smallest convex curve $E_1(\cdot)$ containing the energy curve $E(\cdot)$ using a concavity analysis algorithm [23], and exploiting these two curves, we derive an initialization threshold t_1, which is close to the optimal one. The proposed technique is described in Table I.

Each neuron in the network is initialized by considering this automatically derived initialization threshold value t_1. When the network reaches a stable state, it implicitly generates a change detection map.

TABLE I
ALGORITHM FOR AUTOMATICALLY DERIVING THE INITIALIZATION THRESHOLD

Phase 1: Generate the smallest convex curve $E_1(.)$ containing the energy curve $E(.)$
Step 1: Initialize $k = 0$;
Step 2: While $k \neq L$ (L is the maximum gray value of D)
Step 3: For $i = k + 1$ to L
Step 4: Compute the gradient (slope) of the line passing through the points $(k, E(k))$ and $(i, E(i))$.
Step 5: End For
Step 6: Find out a point $(x, E(x))$, $k < x \leq L$, such that the slope of the line passing through the points $(k, E(k))$ and $(x, E(x))$ is maximum
Step 7: Join the two points $(k, E(k))$ and $(x, E(x))$ by a straight line. This line is a part of the convex curve $E_1(.)$ from threshold value k to x.
Step 8: Reset $k = x$.
Step 9: End While
Phase 2: Derive the initialization threshold value t_1
Step 10: Select the maximum energy value point $(z, E(z))$ in energy curve $E(.)$ (see Fig. 4).
Step 11: Select t_2, so that $\{E_1(t_2) - E(t_2)\} = \max_i\{E_1(i) - E(i)\}$, $z \leq i \leq L$.
Step 12: Select the initialization threshold value t_1, at the intersection between the straight line connecting $(z, E(z))$ and $(t_2, E(t_2))$ and the straight line parallel to the abscissa and passing through minimum energy value $E(L)$ (see Fig. 4).
Step 13: Stop.

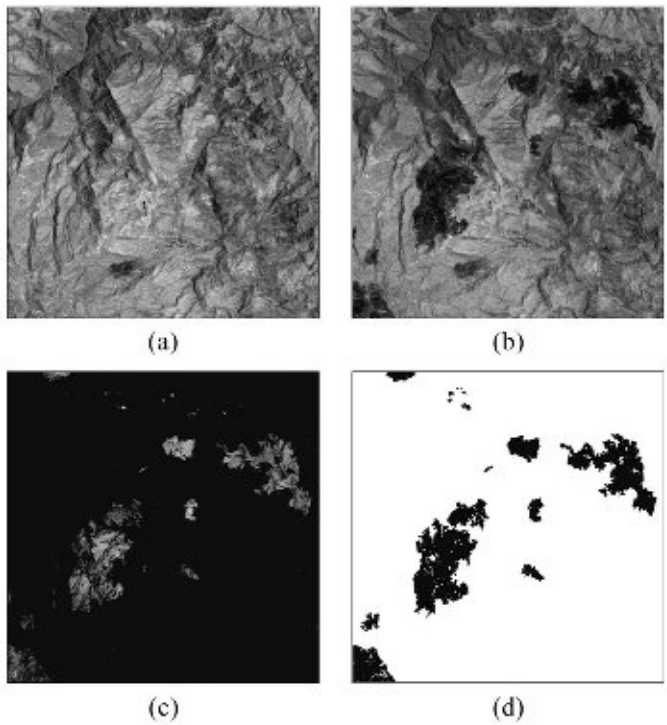

Fig. 5. Images of Mexico. (a) Band 4 of the Landsat ETM+ image acquired in April 2000, (b) band 4 of the Landsat ETM+ image acquired in May 2002, (c) corresponding difference image generated by CVA technique, and (d) reference map of the changed area.

IV. EXPERIMENTAL RESULTS

A. Description of the Experiments

In our experiments, we used two different data sets related to two areas in Mexico and Italy. Four change detection maps were generated for each data set by using four different Hopfield network models (i.e., the maps were produced by the discrete and continuous Hopfield models considering first- and second-order neighborhoods). In the continuous model, the activation function defined in (10) was used for updating the status of the network setting $r = 2$ to have a moderate steepness. It is worth noting that the change detection process is less sensitive to variations of r. On the basis of these results, two different experiments were carried out to test the validity of the proposed technique.

The first experiment aims at evaluating the effectiveness of both the proposed technique and the related initialization algorithm (see Section III-C). To this end, the optimal initialization threshold value t_0 was computed by a manual trial-and-error procedure, i.e., generating the change detection map by initializing the network with different threshold values and computing the corresponding overall change detection error by using the available reference map. The optimal initialization threshold value t_0 corresponds to the minimum overall error. This value and the related error were compared with the value of the initialization threshold t_1 obtained automatically by the proposed approach and the corresponding overall change detection error, respectively.

The second experiment compares the results provided by the proposed technique with the best possible accuracies obtained both manually and with a context-sensitive change detection technique published in the literature [12]. This experiment is aimed at assessing the effectiveness of the proposed technique in terms of change detection error by comparing it with the result obtained by a manual trial-and-error thresholding (MTET) technique. This technique generates a minimum error change detection map under the hypothesis of spatial independence among pixels by finding an optimal decision threshold for D. The optimal decision threshold is obtained by performing a nonautomatic evaluation of the change detection errors versus all possible values of the decision threshold. To prove the effectiveness of the proposed technique, we also compared the change detection error obtained by the proposed approach with that resulting by using the automatic context-sensitive change detection technique presented in [12]. This technique is based on the combined use of the EM algorithm and MRF (we refer to it as EM+MRF technique). Comparisons were carried out in terms of both overall change detection error and number of false alarms (i.e., unchanged pixels identified as changed ones) and missed alarms (i.e., changed pixels categorized as unchanged ones).

B. Experimental Results on Mexico Data Set

The first data set used in the experiments is made up of two multispectral images acquired by the Landsat Enhanced Thematic Mapper Plus (ETM+) sensor of the Landsat-7 satellite in an area of Mexico in April 2000 and May 2002. From the entire available Landsat scene, a section of 512 × 512 pixels has been selected as test site. As an example of the images used, Fig. 5(a) and (b) shows channel 4 of the 2000 and 2002 images, respectively. Between the two aforementioned acquisition dates, a fire destroyed a large portion of the vegetation in the considered region. To be able to make a quantitative evaluation of the effectiveness of the proposed approach, a reference map

TABLE II
CHANGE DETECTION RESULTS OBTAINED BY THE PROPOSED APPROACH (CONSIDERING FOUR DIFFERENT NETWORK MODELS) INITIALIZED BY THE OPTIMAL INITIALIZATION THRESHOLD t_0 AND THE AUTOMATICALLY DERIVED INITIALIZATION THRESHOLD t_1 (BAND 4, MEXICO DATA SET)

Network Model	Initialization threshold		Missed Alarms	False Alarms	Overall Error
	t_0	t_1			
1st Order Discrete	34	-	1252	1640	2892
	-	33	1102	1802	2904
1st Order Continuous	34	-	1035	1554	2589
	-	31	660	2157	2817
2nd Order Discrete	31	-	1010	1740	2750
	-	27	608	2404	3012
2nd Order Continuous	30	-	733	2211	2944
	-	28	558	2707	3265

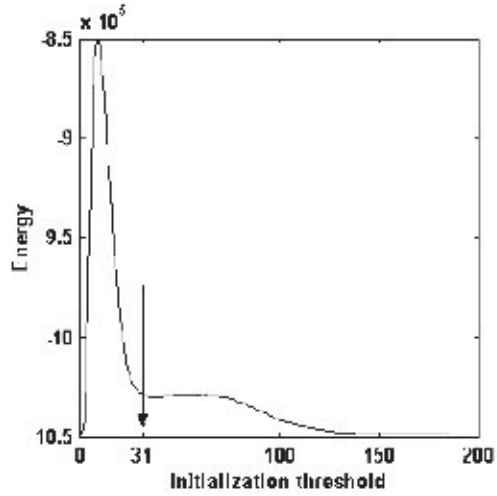

Fig. 6. Behavior of the energy value versus the initialization threshold value (continuous Hopfield model with first-order neighborhood) for band 4, Mexico data set. The initialization threshold value detected by the proposed approach is pointed out by an arrow.

TABLE III
OVERALL ERROR, MISSED ALARMS, AND FALSE ALARMS RESULTING FROM THE PROPOSED CONTEXT-BASED TECHNIQUE (WITH FIRST-ORDER CONTINUOUS MODEL), THE MTET TECHNIQUE, AND THE CONTEXT-SENSITIVE TECHNIQUE BASED ON EM ALGORITHM AND MRF (BAND 4, MEXICO DATA SET)

Techniques	Missed Alarms	False Alarms	Overall Error
MTET	2404	2187	4591
Proposed (1st Order Continuous)	660	2157	2817
EM–MRF ($\beta = 1.5$)	946	2257	3203

was manually defined [see Fig. 5(d)] according to a detailed visual analysis of both the available multitemporal images and the difference image [see Fig. 5(c)]. Different color composites of the aforementioned images were used to highlight all the portions of the changed area in the best possible way. This procedure resulted in a reference map containing 25 599 changed and 236 545 unchanged pixels. Experiments were carried out to produce, in an automatic way, a change detection map as similar as possible to the reference map that represents the best result obtainable with a time-consuming manual procedure.

An analysis of the behaviors of the histogram of multitemporal images did not reveal any significant difference due to light and atmospheric conditions at the acquisition dates. Therefore, no radiometric correction algorithms were applied. The 2002 image was registered on the 2000 one using 12 ground control points. The procedure led to a residual average misregistration error on ground control points of about 0.3 pixels.

First of all, we performed some trials to determine the most effective spectral bands for detecting the burned area in the considered data set. On the basis of the results of these trials, we found that band 4 is very effective to locate the burned area, and that band 5 also contains some information about the burned regions. Hence, we generated two difference images using the CVA technique: one is obtained by considering only spectral band 4, whereas the other is generated by considering spectral bands 4 and 5. In this way, we generated two different data sets (with different information) on which the effectiveness of the proposed technique was assessed.

1) Experimental Results on the Difference Image Generated by Band 4: To assess the validity of the proposed initialization technique, in the first experiment, a comparison was carried out between the optimal initialization threshold t_0 (which was derived manually) and the initialization threshold t_1 obtained by the proposed approach. Taking four different types of Hopfield network model (discrete and continuous with first- and second-order neighborhoods), the initialization of each architecture was carried out by considering the aforementioned initialization threshold values. Table II reports the obtained change detection results. From an analysis of the table, one can deduce that the proposed initialization technique provided accurate initialization threshold values as the automatically derived value t_1 is always close to the manually derived optimal value t_0. Fig. 6 shows the behavior of the energy value versus the initialization threshold value for continuous Hopfield model with first-order neighborhood. It also shows the automatically derived threshold value t_1 (31), which is very close to the manually derived optimal threshold value t_0 (34). It is worth noting that the overall change detection errors obtained by initializing the network considering t_1 are close to the errors yielded by the optimal initialization threshold t_0. In particular, by considering the best architecture (first-order continuous model), the proposed technique resulted in an overall change detection error equal to 2817 pixels, which is close to the optimal one (2589 pixels).

In the second experiment, the change detection map produced by the proposed approach was compared with the change detection maps produced by the MTET procedure and the context-sensitive EM+MRF technique (see [12]). Table III shows that the overall error obtained by the proposed method is much smaller than the overall error incurred by the context-insensitive MTET technique. Concerning the error typology, by considering the best architecture, the proposed technique resulted in 660 missed alarms and 2157 false alarms, whereas the MTET procedure involved 2404 missed alarms and 2187 false alarms. For a better understanding of the behavior of the different methods, Fig. 7 depicts the change detection maps produced by them. A visual comparison points out that the proposed approach, due to a proper exploitation of the contextual information, generates a more smooth change detection map compared to the MTET procedure. Table III also presents the best change detection results obtained by the context-sensitive

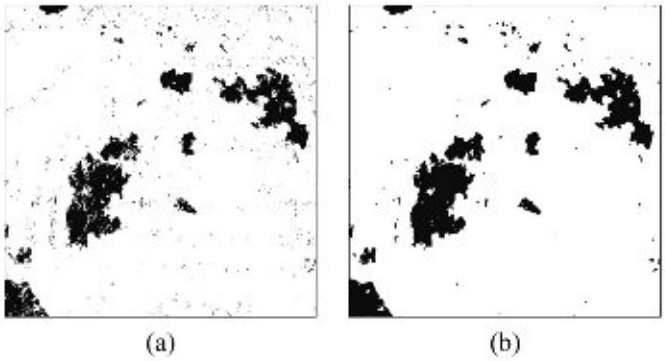

Fig. 7. Change detection maps obtained for the band 4 data set related to the Mexico area by using (a) the MTET technique and (b) the proposed technique (first-order continuous model).

TABLE IV
CHANGE DETECTION RESULTS OBTAINED BY THE PROPOSED APPROACH (CONSIDERING FOUR DIFFERENT NETWORK MODELS) INITIALIZED BY THE OPTIMAL INITIALIZATION THRESHOLD t_0 AND THE AUTOMATICALLY DERIVED INITIALIZATION THRESHOLD t_1 (BANDS 4 AND 5, MEXICO DATA SET)

Network Model	Initialization threshold		Missed Alarms	False Alarms	Overall Error
	t_0	t_1			
1st Order Discrete	45	-	2154	2033	4187
	-	46	2363	1858	4221
1st Order Continuous	45	-	1790	1786	3566
	-	44	1641	2016	3657
2nd Order Discrete	43	-	1820	1433	3253
	-	39	1351	2004	3355
2nd Order Continuous	44	-	1629	1668	3297
	-	40	1086	2407	3493

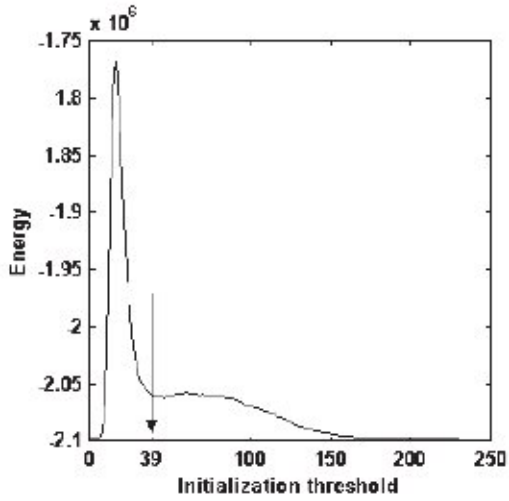

Fig. 8. Behavior of the energy value versus the initialization threshold value (discrete Hopfield model with second-order neighborhood) for bands 4 and 5, Mexico data set. The initialization threshold value detected by the proposed approach is pointed out by an arrow.

TABLE V
OVERALL ERROR, MISSED ALARMS, AND FALSE ALARMS RESULTING FROM THE PROPOSED CONTEXT-BASED TECHNIQUE (WITH SECOND-ORDER DISCRETE MODEL), THE MTET TECHNIQUE, AND THE CONTEXT-SENSITIVE TECHNIQUE BASED ON EM ALGORITHM AND MRF (BANDS 4 AND 5, MEXICO DATA SET)

Techniques	Missed Alarms	False Alarms	Overall Error
MTET	4006	3130	7136
Proposed (2nd Order Discrete)	1351	2004	3355
EM+MRF	1866	898	2764

EM+MRF technique, when the parameter β of MRF [12] was set to 1.5 (this value was defined manually and corresponds to the minimum possible error). From the table, one can see that the overall change detection error obtained by the proposed technique is smaller than the minimum error yielded by the EM+MRF technique. In particular, when adopting the first-order continuous model, the number of missed alarms decreases from 946 to 660, and the number of false alarms decreases from 2257 to 2157. In addition, the proposed technique does not require the optimization of the parameter β, thus, resulting in a more practical tool for operational applications.

2) Experimental Results on the Difference Image Generated by Bands 4 and 5: Concerning the first experiment, Table IV shows the optimal (t_0) and the automatically derived (t_1) initialization thresholds and the corresponding change detection results obtained using the four considered network architectures. From an analysis of these results, it is also possible to observe that in this case the threshold value t_1 (which is automatically derived by the proposed initialization technique) is close to the manually derived optimal threshold value t_0. Fig. 8 depicts the behavior of the energy value versus the initialization threshold value for the discrete Hopfield model with second-order neighborhood [it also shows the automatically derived threshold value t_1 (39), which is very close to the manually derived optimal threshold value t_0 (43)]. From the table, it is observed that the overall change detection errors obtained by initializing the network with t_1 are very close to the optimum results obtained with t_0. As an example, consider the second-order discrete network model where the proposed technique resulted in an overall error of 3355 pixels, whereas the minimum overall error was equal to 3253 pixels.

The results obtained in the second experiment (see Table V) confirm the validity of the presented context-based technique. In particular, considering any of the four network models, the overall change detection error was reduced, as compared with the one incurred when using the manual optimal context-insensitive MTET technique. For example, for the second-order discrete network architecture, the overall error obtained with the proposed context-based technique was equal to 3355 pixels, whereas the error yielded by the MTET technique was equal to 7136 pixels. In greater detail, the number of missed alarms decreased from 4006 to 1351, and the number of false alarms was reduced from 3130 to 2004. Fig. 9 shows the change detection maps produced by the two techniques. A comparison between these two maps points out the capability of the proposed method to exploit the spatiocontextual information for reducing the noise present in the maps. The proposed technique provided an overall accuracy comparable with that yielded by the context-sensitive EM+MRF technique (with the optimal value of the parameter β equal to 1.1). Concerning the error typology, the EM+MRF approach increased the missed alarms from 1351 pixels to 1866 pixels, whereas the false alarms are reduced from 2004 pixels to 898 pixels, decreasing the overall error from 3355 to 2764 pixels.

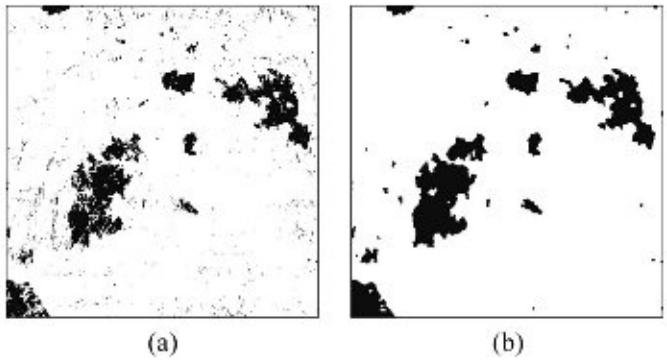

Fig. 9. Change detection maps obtained for the bands 4 and 5 data set related to the Mexico area by using (a) the MTET technique and (b) the proposed technique (second-order discrete model).

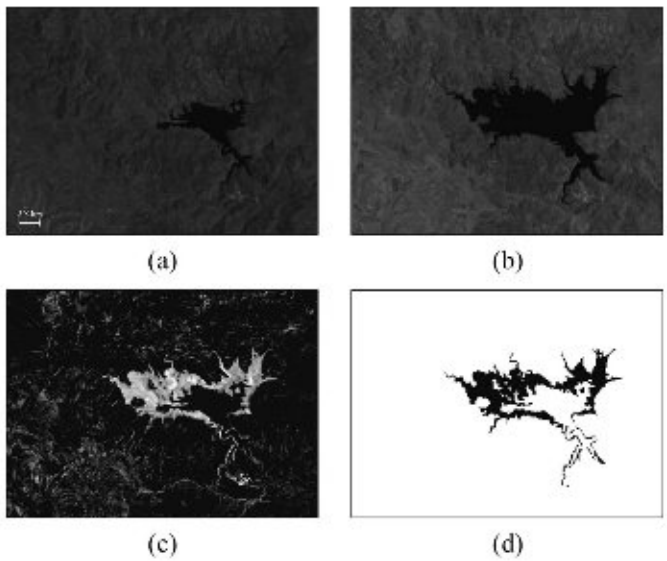

Fig. 10. Images of Sardinia Island, Italy. (a) Band 4 of the Landsat TM image acquired in September 1995, (b) band 4 of the Landsat TM image acquired in July 1996, (c) difference image generated by CVA technique using bands 1, 2, 4, and 5, and (d) reference map of the changed area.

C. Experimental Results on the Sardinia Island Data Set

The second data set used in the experiments was made up of two multispectral images acquired by the Landsat Thematic Mapper (TM) sensor of the Landsat-5 satellite in September 1995 and July 1996. The test site is a section (412 × 300 pixels) of a scene including Lake Mulargia on the Island of Sardinia (Italy). Between the two aforementioned acquisition dates, the water level in the lake increased (see the lower central part of the image). Fig. 10(a) and (b) shows channel 4 of the 1995 and 1996 images. As done for the Mexico data set, also in this case, a reference map was manually defined [see Fig. 10(d)] according to a detailed visual analysis of both the available multitemporal images and the difference image [see Fig. 10(c)]. At the end, 7480 changed and 116 120 unchanged pixels were identified. As histograms did not show any significant difference, no radiometric correction algorithms were applied to the multitemporal images. The images were coregistered with 12 ground control points resulting in an average residual misregistration error of about 0.2 pixels on the ground control points.

TABLE VI
CHANGE DETECTION RESULTS OBTAINED BY THE PROPOSED APPROACH (CONSIDERING FOUR DIFFERENT NETWORK MODELS) INITIALIZED BY THE OPTIMAL INITIALIZATION THRESHOLD t_0 AND THE AUTOMATICALLY DERIVED INITIALIZATION THRESHOLD t_1 (SARDINIA ISLAND DATA SET)

Network Model	Initialization threshold		Missed Alarms	False Alarms	Overall Error
	t_0	t_1			
1st Order Discrete	90	-	862	614	1476
	-	86	667	1065	1732
1st Order Continuous	90	-	1060	455	1515
	-	90	1060	455	1515
2nd Order Discrete	87	-	1193	606	1799
	-	82	1080	852	1932
2nd Order Continuous	86	-	1292	552	1844
	-	83	1187	722	1909

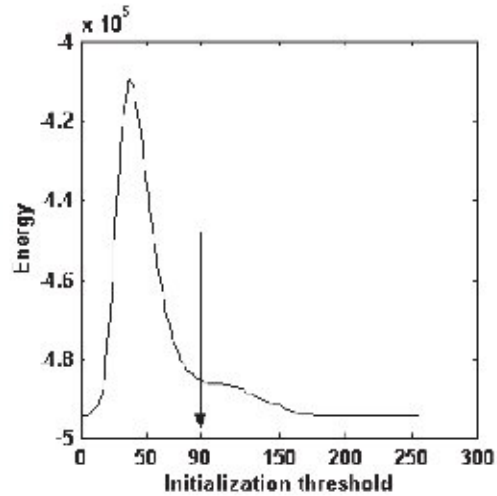

Fig. 11. Behavior of the energy value versus the initialization threshold value (continuous Hopfield model with first-order neighborhood) for Sardinia Island data set. The initialization threshold value detected by the proposed approach is pointed out by an arrow.

Similar experiments as described in Section IV-A were carried out on this data set to further prove the validity of the presented technique. To this end, we applied the CVA technique to spectral bands 1, 2, 4, and 5 of the two multispectral images, as preliminary experiments show that the above channels contain useful information on the changes in water level.

Also in this case, in the first experiment, we considered four Hopfield network architectures. The initialization of each architecture was carried out by considering both the manually derived optimal threshold t_0 and the automatically derived threshold t_1. The corresponding change detection results are reported in Table VI. By analyzing the results displayed in the table, one can deduce that, also in this case, the proposed initialization technique provided a threshold value t_1 that is very close to the optimal initialization threshold t_0. Fig. 11 shows the behavior of the energy value versus the initialization threshold value for continuous Hopfield model with first-order neighborhood. By considering this architecture, the proposed technique incurred an overall error of 1515 pixels, which is equal to that of the optimal one (as t_0).

TABLE VII
OVERALL ERROR, MISSED ALARMS, AND FALSE ALARMS RESULTING FROM THE PROPOSED CONTEXT-BASED TECHNIQUE (WITH FIRST-ORDER CONTINUOUS MODEL), THE MTET TECHNIQUE, AND THE CONTEXT-SENSITIVE TECHNIQUE BASED ON EM ALGORITHM AND MRF (SARDINIA ISLAND DATA SET)

Techniques	Missed Alarms	False Alarms	Overall Error
MTET	1015	875	1890
Proposed (1st Order Continuous)	1060	455	1515
EM+MRF	592	1108	1700

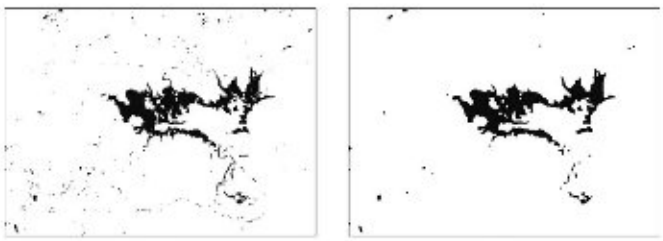

(a) (b)

Fig. 12. Change detection maps obtained for the Sardinia Island data set by using (a) the MTET technique and (b) the proposed technique (first-order continuous model).

By analyzing the results of the second experiment shown in Table VII, one can conclude that the overall change detection error obtained by the proposed context-sensitive technique is slightly better than the overall error produced by the MTET procedure. In particular, the overall change detection error obtained with the proposed technique is equal to 1932 pixels in the worst case (considering the second-order discrete model) and equal to 1515 pixels in the best case (considering the first-order continuous model). This error should be compared with an overall error of 1890 pixels produced by the MTET technique. Fig. 12 shows the change detection maps produced by the two techniques for visual comparison. Table VII shows that the proposed context-sensitive technique provided better accuracy than the best result yielded by the context-sensitive EM+MRF technique. Considering the first-order continuous network architecture, the proposed context-sensitive approach incurred an overall error equal to 1515 pixels (1060 missed alarms and 455 false alarms), whereas the overall error for the context-sensitive EM+MRF approach was equal to 1700 pixels (592 missed alarms and 1108 false alarms).

V. DISCUSSION AND CONCLUSION

In this paper, an unsupervised and automatic context-sensitive technique for change detection in multitemporal images has been proposed. The technique models the spatial correlation between neighboring pixels in the difference image by using a Hopfield neural network implemented according to a specific architecture, where connections between neurons are properly defined. In greater detail, the architecture of the network represents the difference image structure by associating a neuron to each pixel; this allows to easily define the spatial neighborhood of each neuron and, accordingly, to properly define the weights of the connections among different units (pixels). On the basis of this architecture, an energy function associated with the state of the network is defined that models the information present in both the radiance of the difference image pixels and the spatial context of each unit. The state of the network is initialized according to a simple thresholding of the difference image; the threshold value is derived according to a heuristic yet effective threshold selection procedure.

The presented technique shows the following advantages with respect to the reference context-sensitive method based on EM and MRF (EM+MRF) model presented in [12]: 1) it is distribution free, i.e., it does not require any explicit assumption on the statistical model of the distributions of classes of changed and unchanged pixels and 2) it does not require the setting of any input parameter (except the definition of the neighborhood order, like in MRF) and, thus, is completely automatic (the EM+MRF technique requires the definition of the regularization parameter that tunes the effect of the spatial context information in the energy function to be optimized). The main disadvantage of the presented method is related to the second advantage, i.e., it consists of the fact that, in the current implementation, it is not possible to tune the influence of the spatial context information in the minimization of the energy function. However, this is a reasonable drawback considering the important advantage of having no parameters to set as input to the algorithm.

Experimental results obtained on different real multitemporal data sets confirm the effectiveness of the proposed approach, which significantly outperforms the standard optimal-manual context-insensitive technique and provides an overall change detection error comparable (in some cases, slightly smaller; in other cases, slightly higher) to the one achieved with the context-sensitive EM+MRF technique.

As a final remark, it is worth noting that, as the considered Hopfield architecture has a small number of connections (each neuron is connected only to its neighboring neurons and not to all the neurons in the network), the proposed method is quite fast (the convergence is reached in less than 60 iterations).

ACKNOWLEDGMENT

The authors would like to thank the anonymous referees for their constructive criticism. This work has been carried out in the framework of the India–Trento Program for Advanced Research.

REFERENCES

[1] A. Singh, "Digital change detection techniques using remotely sensed data," *Int. J. Remote Sens.*, vol. 10, no. 6, pp. 989–1003, 1989.
[2] J. A. Richards and X. Jia, *Remote Sensing Digital Image Analysis*, 4th ed. Berlin, Germany: Springer-Verlag, 2006.
[3] J. Cihlar, T. J. Pultz, and A. L. Gray, "Change detection with synthetic aperture radar," *Int. J. Remote Sens.*, vol. 13, no. 3, pp. 401–414, 1992.
[4] L. Bruzzone and S. B. Serpico, "An iterative technique for the detection of land-cover transitions in multitemporal remote-sensing images," *IEEE Trans. Geosci. Remote Sens.*, vol. 35, no. 4, pp. 858–867, Jul. 1997.
[5] L. Bruzzone and D. Fernàndez Prieto, "An adaptive parcel-based technique for unsupervised change detection," *Int. J. Remote Sens.*, vol. 21, no. 4, pp. 817–822, 2000.
[6] S. Gopal and C. Woodcock, "Remote sensing of forest change using artificial neural networks," *IEEE Trans. Geosci. Remote Sens.*, vol. 34, no. 2, pp. 398–404, Mar. 1996.
[7] T. Hame, I. Heiler, and J. S. Miguel-Ayanz, "An unsupervised change detection and recognition system for forestry," *Int. J. Remote Sens.*, vol. 19, no. 6, pp. 1079–1099, 1998.

[8] P. S. Chavez, Jr. and D. J. MacKinnon, "Automatic detection of vegetation changes in the southwestern United States using remotely sensed images," *Photogramm. Eng. Remote Sens.*, vol. 60, no. 5, pp. 1285–1294, 1994.
[9] K. R. Merril and L. Jiajun, "A comparison of four algorithms for change detection in an urban environment," *Remote Sens. Environ.*, vol. 63, no. 2, pp. 95–100, 1998.
[10] T. Fung, "An assessment of TM imagery for land-cover change detection," *IEEE Trans. Geosci. Remote Sens.*, vol. 28, no. 4, pp. 681–684, Jul. 1990.
[11] D. M. Muchoney and B. N. Haack, "Change detection for monitoring forest defoliation," *Photogramm. Eng. Remote Sens.*, vol. 60, no. 10, pp. 1243–1251, 1994.
[12] L. Bruzzone and D. Fernàndez Prieto, "Automatic analysis of the difference image for unsupervised change detection," *IEEE Trans. Geosci. Remote Sens.*, vol. 38, no. 3, pp. 1171–1182, May 2000.
[13] J. R. G. Townshend and C. O. Justice, "Spatial variability of images and the monitoring of changes in the normalized difference vegetation index," *Int. J. Remote Sens.*, vol. 16, no. 12, pp. 2187–2195, 1995.
[14] A. P. Dempster, N. M. Laird, and D. B. Rubin, "Maximum likelihood from incomplete data via the EM algorithm," *J.R. Stat. Soc.*, vol. 39, no. 1, pp. 1–38, 1977.
[15] Y. Bazi, L. Bruzzone, and F. Melgani, "An unsupervised approach based on the generalized Gaussian model to automatic change detection in multitemporal SAR images," *IEEE Trans. Geosci. Remote Sens.*, vol. 43, no. 4, pp. 874–887, Apr. 2005.
[16] L. Bruzzone and D. Fernàndez Prieto, "An adaptive semiparametric and context-based approach to unsupervised change detection in multitemporal remote-sensing images," *IEEE Trans. Image Process.*, vol. 11, no. 4, pp. 452–466, Apr. 2002.
[17] A. Ghosh, N. R. Pal, and S. K. Pal, "Object background classification using Hopfield type neural network," *Int. J. Pattern Recognit. Artif. Intell.*, vol. 6, no. 5, pp. 989–1008, 1992.
[18] S. Haykin, *Neural Networks: A Comprehensive Foundation*. Singapore: Pearson Education, 2003. Fourth Indian Reprint.
[19] S. V. B. Aiyer, M. Niranjan, and F. Fallside, "A theoretical investigation into the performance of the Hopfield model," *IEEE Trans. Neural Netw.*, vol. 1, no. 2, pp. 204–215, Jun. 1990.
[20] J. J. Hopfield, "Neural networks and physical systems with emergent collective computational abilities," *Proc. Nat. Acad. Sci., U.S.A.*, vol. 79, no. 8, pp. 2554–2558, Apr. 1982.
[21] ——, "Neurons with graded response have collective computational properties like those of two state neurons," *Proc. Nat. Acad. Sci., U.S.A.*, vol. 81, no. 10, pp. 3088–3092, May 1984.
[22] S. K. Pal and D. Dutta Majumdar, *Fuzzy Mathematical Approach to Pattern Recognition*. New York: Halsted, 1986.
[23] A. Rosenfeld and P. De La Torre, "Histogram concavity analysis as an aid in threshold selection," *IEEE Trans. Syst., Man, Cybern.*, vol. SMC-13, no. 3, pp. 231–235, Mar. 1983.

Susmita Ghosh received the B.Sc. degree (with honors) in physics and the B.Tech. degree in computer science and engineering from the University of Calcutta, Kolkata, India, in 1988 and 1991, respectively, the M.Tech. degree in computer science and engineering from the Indian Institute of Technology, Bombay, in 1993, and the Ph.D. degree in engineering from Jadavpur University, Kolkata, in 2004.

In May 1999, she was with the Institute of Automation, Chinese Academy of Sciences, Beijing, with a CIMPA (France) fellowship. She has also visited various universities/academic institutes for collaborative research and delivered lectures in different countries, including Australia, Italy, and Japan. She was a Lecturer with the Department of Computer Science and Engineering, Jadavpur University, during 1997–2002. She is currently a Reader at the same department. Her research interests include genetic algorithms, neural networks, image processing, pattern recognition, soft computing, and remotely sensed image analysis.

Lorenzo Bruzzone (S'95–M'98–SM'03) received the Laurea Specialistica (M.S.) degree (*summa cum laude*) in electronic engineering and the Ph.D. degree in telecommunications from the University of Genoa, Genoa, Italy, in 1993 and 1998, respectively.

From 1998 to 2000, he was a Postdoctoral Researcher with the University of Genoa. From 2000 to 2001, he was an Assistant Professor with the University of Trento, Trento, Italy, where he was an Associate Professor from 2001 to 2005. Since March 2005, he has been a Full Professor of telecommunications with the University of Trento, where he currently teaches remote sensing, pattern recognition, and electrical communications. He is currently the Head of the Remote Sensing Laboratory, Department of Information and Communication Technology, University of Trento. He is the author (or coauthor) of more than 150 scientific publications, including journals, book chapters, and conference proceedings. His current research interests are in the area of remote sensing image processing and recognition (analysis of multitemporal data, feature selection, classification, regression, data fusion, and machine learning). He conducts and supervises research on these topics within the frameworks of several national and international projects. Since 1999, he has been appointed Evaluator of project proposals for the European Commission. He is a Referee for many international journals and has served on the scientific committees of several international conferences.

Dr. Bruzzone ranked first place in the Student Prize Paper Competition of the 1998 IEEE International Geoscience and Remote Sensing Symposium (Seattle, July 1998). He received recognition of the IEEE TRANSACTIONS ON GEOSCIENCE AND REMOTE SENSING Best Reviewers in 1999 and was a Guest Editor of a Special Issue of the IEEE TRANSACTIONS ON GEOSCIENCE AND REMOTE SENSING on the subject of the analysis of multitemporal remote sensing images (November 2003). He was the General Chair and Cochair of the First and Second IEEE International Workshop on the Analysis of Multitemporal Remote Sensing Images. Since 2003, he has been the Chair of the SPIE Conference on Image and Signal Processing for Remote Sensing. He is an Associate Editor of the IEEE TRANSACTIONS ON GEOSCIENCE AND REMOTE SENSING. He is a member of the Scientific Committee of the India–Italy Center for Advanced Research. He is also a member of the International Association for Pattern Recognition and of the Italian Association for Remote Sensing (AIT).

Swarnajyoti Patra received the B.Sc. degree in computer science and the M.C.A. degree from Vidyasagar University, Midnapore, India, in 1999 and 2003, respectively.

He is currently a Research Scholar under the India–Trento Program for Advanced Research—Telecommunications project with the Department of Computer Science and Engineering, Jadavpur University, Kolkata, India. His research interests include pattern recognition, evolutionary computation, neural networks, and remote sensing image analysis.

Francesca Bovolo (S'05–M'07) received the Laurea (B.S.) and Laurea Specialistica (M.S.) degrees in telecommunication engineering (*summa cum laude*) and the Ph.D. degree in communication and information technologies from the University of Trento, Trento, Italy, in 2001, 2003, and 2006, respectively.

She currently holds a postdoctoral position at the Pattern Recognition and Remote Sensing Group, Department of Information and Communication Technologies, University of Trento. Her main research activity is in the area of remote-sensing image processing; in particular, her interests are related to the analysis of multitemporal data and to change detection in multispectral and SAR images. She conducts research on these topics within the frameworks of several national and international projects. She is a referee for the *International Journal of Remote Sensing*, the *Photogrammetric Engineering and Remote Sensing*, and the *Remote Sensing of Environment*.

Dr. Bovolo served on the Scientific Committee of the SPIE International Conference on "Signal and Image Processing for Remote Sensing XI" (Stockholm, Sweden, September 2006) and is a member of the Scientific Committee of the IEEE Fourth International Workshop on the Analysis of Multi-Temporal Remote Sensing Images (MultiTemp 2007). She is a referee for the IEEE TRANSACTIONS ON GEOSCIENCE AND REMOTE SENSING. She ranked First Place in the Student Prize Paper Competition of the 2006 IEEE International Geoscience and Remote Sensing Symposium (Denver, August 2006).

Ashish Ghosh received the B.E. degree in electronics and telecommunications from Jadavpur University, Kolkata, India, in 1987, and the M.Tech. and Ph.D. degrees in computer science from the Indian Statistical Institute, Kolkata, in 1989 and 1993, respectively.

He is currently a Professor with the Machine Intelligence Unit, Indian Statistical Institute, and is a member of the founding team that established a National Center for Soft Computing Research at the Indian Statistical Institute in 2004 with funding from the Department of Science and Technology, Government of India. He has been selected as an Associate of the Indian Academy of Sciences, Bangalore, in 1997. From October 1995 to March 1997, he visited the Osaka Prefecture University, Sakai, Japan, with a postdoctoral fellowship. He also visited Hannan University, Matsubara, Japan, during September–October 1997 and September–October 2004 as a Visiting Faculty and again during February–April 2005 as a Visiting Professor with a fellowship from the Japan Society for Promotion of Sciences. In May 1999, he was with the Institute of Automation, Chinese Academy of Sciences, Beijing, with a CIMPA (France) fellowship. During January–April 2000, he was with the German National Research Center for Information Technology, Sankt Augustin, with a German Government (DFG) fellowship. During October–December 2003, he was a Visiting Professor with the University of California, Los Angeles. His visits to the University of Trento, Trento, Italy, and the University of Palermo, Palermo, Italy, during May–June 2004 and March–April 2006 were in connection with collaborative international projects. He has also visited various universities/academic institutes and delivered lectures in different countries, including South Korea, Poland, and The Netherlands. He has already published about 100 research papers in internationally reputed journals and referred conferences and has edited six books. His research interests include pattern recognition and machine learning, data mining, image analysis, remotely sensed image analysis, soft computing, fuzzy sets and uncertainty analysis, neural networks, evolutionary computation, and bioinformatics. He is a Guest Editor for various international journals.

Dr. Ghosh received the prestigious and most coveted Young Scientists Award in engineering sciences from the Indian National Science Academy in 1995 and Young Scientists Award in computer science from the Indian Science Congress Association in 1992.